



Physics-based plasticity model incorporating microstructure changes for severe plastic deformation



Ziyad Zenasni^a, Mohamed Haterbouch^a, Zoubir Atmani^b, Samir Atlati^c,
Mohammed Zenasni^c, Khalid Nasri^{c,d,*}, Omar Oussouaddi^e

^a Équipe de mécanique et ingénierie intégrée (M2I), ENSAM, Université Moulay-Ismaïl, Meknès, Morocco

^b Centre de recherche des Écoles de Saint-Cyr Coëtquidan, École militaire de Coëtquidan, 56380 Guer, France

^c Équipe de mécanique et calcul scientifique (EMCS), ENSA, Université Mohammed-I^{er}, Oujda, Morocco

^d SCD Laboratory, Faculty of Sciences, University Abdelmalek-Essaadi, 93030 Tetouan, Morocco

^e Laboratoire d'étude des matériaux avancés et applications (EM2A), Faculté des sciences, Université Moulay-Ismaïl, Meknès, Morocco

ARTICLE INFO

Article history:

Received 20 February 2019

Accepted 1 June 2019

Available online 9 July 2019

Keywords:

Plasticity
Strain jump
Dislocation density
Mechanical threshold
Cell size
Machining

ABSTRACT

During machining processes, materials undergo severe deformations that lead to different behavior than in the case of slow deformation. The microstructure changes, as a consequence, affect the materials properties and therefore influence the functionality of the component. Developing material models capable of capturing such changes is therefore critical to better understand the interaction process–materials. In this paper, we introduce a new physics model associating Mechanical Threshold Stress (MTS) with Dislocation Density (DD) models. The modeling and the experimental results of a series of large strain experiments on polycrystalline copper (OFHC) involving sequences of shear deformation and strain rate (varying from quasi-static to dynamic) are very similar to those observed in processes such as machining. The Kocks–Mecking model, using the mechanical threshold stress as an internal state variable, correlates well with experimental results and strain rate jump experiments. This model was compared to the well-known Johnson–Cook model that showed some shortcomings in capturing the strain jump. The results show a high effect of rate sensitivity of strain hardening at large strains. Coupling the mechanical threshold stress dislocation density (MTS–DD), material models were implemented in the Abaqus/Explicit FE code. The model shows potentialities in predicting an increase in dislocation density and a reduction in cell size. It could ideally be used in the modeling of machining processes.

© 2019 Académie des sciences. Published by Elsevier Masson SAS. All rights reserved.

1. Introduction

During shaping operations, the material is generally subjected to severe deformation conditions [1–3]. The strain rate suddenly changes from a quasi-static to a dynamic state. These conditions of deformation are accompanied by a change in the microstructure, and therefore influence the mechanical properties of the materials. The most representative models in the literature are often phenomenological, such as the model of JC. In this article, we introduce an original MTS–DD physical

* Corresponding author at: Équipe de mécanique et calcul scientifique (EMCS), ENSA, Université Mohammed-I^{er}, Oujda, Morocco.
E-mail address: khalid.nasri@uae.ac.ma (K. Nasri).

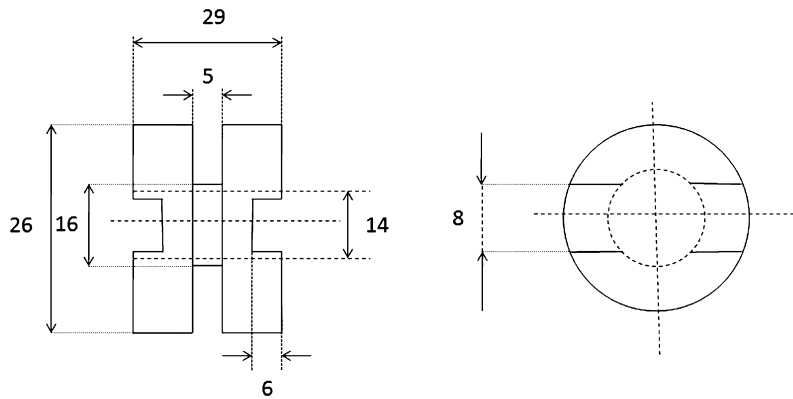


Fig. 1. Geometry of the thin-walled tubes used. The dimensions are in mm.

model that aims to give a physical meaning to the phenomena that accompany plastic deformation under severe conditions (large deformations, high strain rate...).

The understanding of deformation behavior over a wide range of temperature and strain rates is necessary for many engineering application. Almost all experimental studies on strain rate effects have concentrated on instantaneous rate sensitivity at relatively small strains [4]. Moreover, many researchers have performed a series of experiments at constant strain rate or constant temperature. However, accounting for complex paths of deformation, temperature, and strain rate is an important requirement of constitutive laws for large-strain problems [5,6]; in this paper, we will be only interested in the strain-rate history effects at large strain in the case of polycrystalline copper.

An advantage of strain rate sequence experiments is their capability of imposing a rate change within a short period of time. The first experiments involving dynamic strain rate were conducted in compression on aluminum by Lindholm [7,8]. Many investigators have examined the effects of strain rate on copper, and recent reviews can be found in Mao et al. [9], Zhang et al. [10], Chen et al. [11], Huang et al. [12], Jiang et al. [13], Senseny [14], Tanner et al. [15,16]. They observed that the transient flow stress remains between the two constant strain rate curves and approaches the higher-rate curve.

Another challenge in modeling metals is to understand how their microstructure changes during strain rate jump. The dislocation density model was developed by Estrin et al. [17]; it consists of a set of differential equations to evaluate the dislocation density evolution rates, and they applied it to grain refinement assessment in the equal channel angular processing (ECAP) of copper. Also, Estrin et al. [18,19], Lee et al. [20] and Lemiale et al. [21] have used this model to predict the evolution of the microstructure and texture in severe plastic deformation by the ECAP process. More recently, Bacca et al. [22] proposed a new microstructure model estimating the grain size at severe plastic deformation and applied it to the simulation, using FE modeling, of machining Aluminum alloy Al6061-T6. The capability of a particular model is estimated based on its prediction potential from actual measured experimental data that is obtained under the same loading condition, and also for conditions that have not been determined experimentally.

The present paper also focuses on the multi-physics and multi-scale modeling of the behavior of metallic oxygen-free high conductivity (OFHC) copper under different strain rates. To this aim, the MTS physics model is coupled with the dislocation density model (DD) and implemented in the Abaqus software by the VUMAT subroutine using a FORTRAN code. This code has the advantage to be able to perform the simulation analysis of the grains size during extreme dynamic loading.

The paper is organized as follows. The first section describes the experimental procedures used to evaluate the behavior of an OFHC Cu metallic material under different strain rates. The second one highlights the governing equations of the Johnson–Cook model and of Mechanical Threshold Stress (MTS). The Dislocation Density model is also recalled in this section. In the last one, the experimental results are presented, and the capability of the two constitutive models is discussed. Finally, section 5 presents our conclusions.

2. Experimental technique

Torsion experiments at room temperature were conducted on a thin-walled tubular specimen of polycrystalline copper (99.96% pure) at two different nominal strain rates and at large shear strains.

2.1. Quasi-static loading

The quasi static torsion test consists of a thin-walled tubular specimen that is held fixed at one end and twisted at the other using a universal closed-loop testing machine; in that way, the gauge length of the specimen is under a state of pure shear. The specimen geometry is illustrated in Fig. 1. This testing machine is equipped with a digital system of data acquisition and can reach angular velocities ω of about 35°/s and a rotation angle $\varphi_{\max} = 110^\circ$, which corresponds to

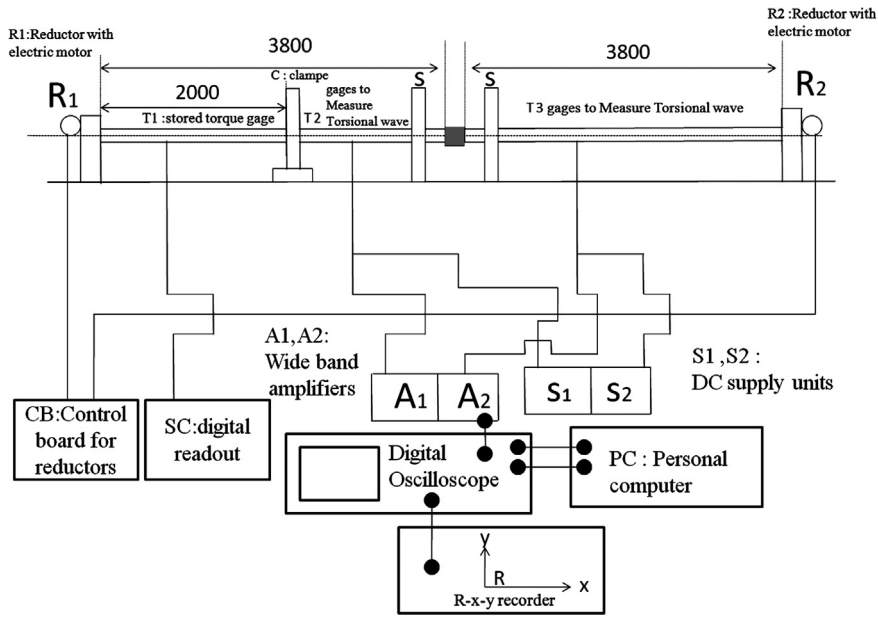


Fig. 2. Split Hopkinson Tensional Bar (SHTB).

the maximum nominal strain. $\Gamma_{max} \cong 3$. The load capacity of the machine is 150 N·m. Experiments were performed at the nominal strain rate $\dot{\Gamma}_{max} \cong 10^{-3} \text{ s}^{-1}$.

2.2. Dynamic loading

The high-strain-rate experiments were performed at the nominal strain rate $\dot{\Gamma}_{max} \cong 350 \text{ s}^{-1}$ using a modified Split Hopkinson Tensional Bar (SHTB) (Fig. 2) apparatus developed by Zenasni et al. [23]. In this technique, a tubular specimen is sandwiched between two bars, known as the incident and transmitted bars. The specimen is loaded by an elastic tensional stress pulse propagated along the incident and transmitted bars. The loading pulse is produced by the sudden release of the stored torque by the clamp C.

The torque is stored on the left side of the incident bar by pre-twisting the clamp part of the bar using an electric motor and a redactor R_1 . Upon release of the clamp, the torsional incident wave $\gamma_I(t)$ of constant amplitude propagates down along the incident bar in the specimen. A part of the incident wave is reflected as the reflected wave $\gamma_R(t)$ and a part is transmitted to the transmitter bar as the transmitted wave $\gamma_T(t)$. All three waves are detected by two four-arm electric resistance strain gage bridges T_2 and T_3 . The electric signals are recorded with a digital oscilloscope DO and stored on the hard disc of a computer for further analysis. Since the maximum nominal shear strain is limited with the SHTB technique to $\Gamma \cong 0.4$, one specimen has to be consecutively loaded from six to eight times to reach the desired large strain $\Gamma \cong 2.5$. For every segment of the dynamic test, the incident, reflected, and transmitted waves were analyzed by a computer providing the constitutive segment of the dynamic curve $(\Gamma, \tau(\Gamma))$. The shear strain and shear stress in the specimen can at any time be determined after some calculation based on the theory of elastic wave propagation in bars. The shear strain is given by:

$$\Gamma(t) = \frac{C_0 r_m}{LR} \int_0^t (\gamma_I - \gamma_R - \gamma_T) dt \tag{2.1}$$

where C_0 is the longitudinal wave propagation and R is the radius of the bar. L and r_m are the length and the mean radius of the specimen, respectively. The shear stress, assumed uniform, is given by

$$\tau(t) = \frac{GR^3}{8r_m e} (\gamma_I + \gamma_R + \gamma_T) \tag{2.2}$$

where G is the shear modulus and e is the thickness of the tubular specimen.

3. Modeling numerical analysis

We have considered at first the case of a simple shear test. Comparing the experimental results of our shear tests on OFHC copper at different strain rates with the numerical results, we check the implementation of the MTS model for this loading case. The relationship between the nominal shear rate $\dot{\Gamma}$ and the applied velocity V is:

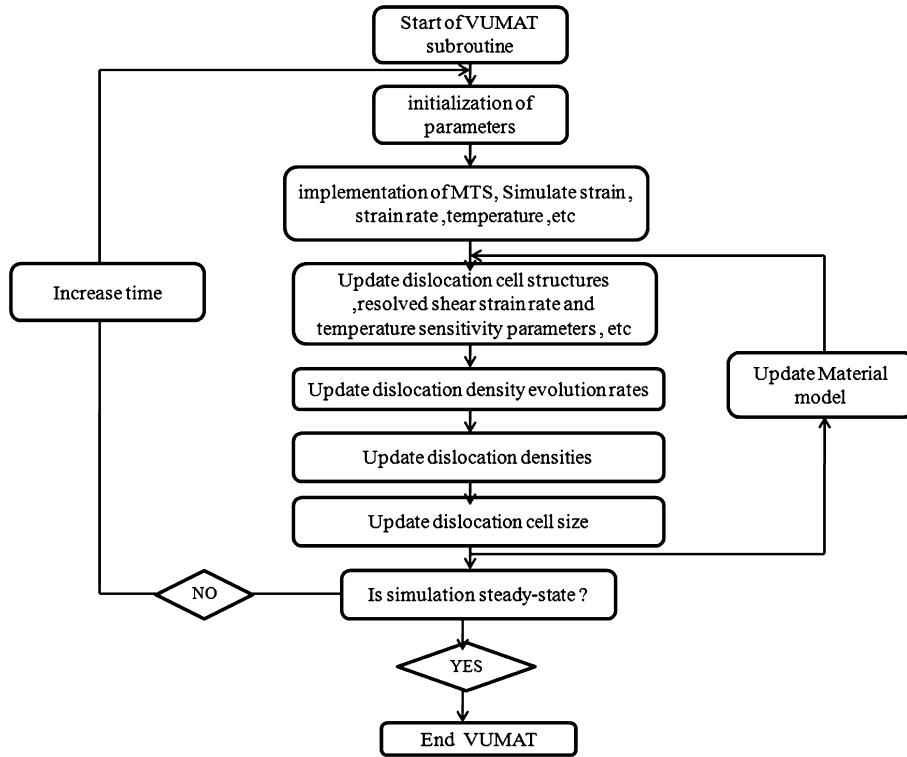


Fig. 3. Flowchart of the implementation of the coupled MTS-DD model with user subroutine VUMAT in Abaqus/Explicit.

$$\dot{\Gamma} \approx \frac{V}{L} \quad (3.1)$$

Quadrilateral, four-node, linearly interpolated elements with automatic hourglass control and reduced integration were used. The MTS model, dedicated to representing the thermoviscoplastic behavior of the material during deformation, is implemented, in association with the DD model, dedicated to predicting the microstructure change in the specimen, via the user material VUMAT written in FORTRAN of the Abaqus/Explicit software. Fig. 3 shows the main steps of the implementation procedure of the coupled MTS-DD model.

We assume the material to be incompressible and isotropic. The inelastic behavior is described using the finite strain version of the J_2 flow theory. The total strain rate is decomposed into its elastic and plastic parts as:

$$\dot{\boldsymbol{\epsilon}} = \dot{\boldsymbol{\epsilon}}^e + \dot{\boldsymbol{\epsilon}}^p \quad (3.2)$$

The elastic deformation rate is governed by Hooke's law, Eq. (3.2), and the inelastic one is governed by the rate equation (3.5) or (3.6)–(3.7).

$$\dot{\boldsymbol{\sigma}} = 2\mu_L \dot{\boldsymbol{\epsilon}}^e + \lambda_L \text{Tr}(\dot{\boldsymbol{\epsilon}}^e) \mathbf{I} \quad (3.3)$$

Moreover, μ_L and λ_L are the Lamé constants, which can be expressed by Young's modulus, E , and Poisson's ratio, ν :

$$\mu_L = \frac{E}{2(1+\nu)}, \quad \lambda_L = \nu \frac{E}{(1+\nu)(1-2\nu)} \quad (3.4)$$

The plastic strain rate is given by the J_2 flow theory:

$$\dot{\boldsymbol{\epsilon}}^p = \frac{3}{2} \frac{\mathbf{S}}{\sigma_e} \dot{\boldsymbol{\epsilon}}^p \quad (3.5)$$

where \mathbf{S}_{ij} is the deviator part of the stress tensor, σ_e and $\dot{\boldsymbol{\epsilon}}^p$ represent the effective stress and the effective plastic strain rate, respectively given by:

$$\sigma_e = \sqrt{\frac{3}{2} \mathbf{S} : \mathbf{S}} \quad \dot{\boldsymbol{\epsilon}}^p = \sqrt{\frac{2}{3} \dot{\boldsymbol{\epsilon}}^p : \dot{\boldsymbol{\epsilon}}^p} \quad (3.6)$$

The accumulated plastic deformation is defined by:

$$\bar{\varepsilon}^P = \int_0^t \sqrt{\frac{2}{3} \dot{\varepsilon}^P : \dot{\varepsilon}^P} dt \quad (3.7)$$

The physical properties of copper are depicted in Table 1.

Table 1
Physical properties of the material [20].

Property	E [GPa]	G [GPa]	ν	ρ [kg/m ³]	T_m [K]	C_v [J/kg·K]
Copper	127.72	46.31	0.351	8960	1356	385

The material behavior is assumed to be described by two constitutive models: the Johnson–Cook model and the MTS–DD model (Tables 2 and 3).

Table 2
JC flow stress parameters of copper [21].

Parameters	A [MPa]	B [MPa]	n	C	M	T_{ref} [K]	T_m [K]	$\dot{\varepsilon}_0$ [s ⁻¹]
Copper	90	292	0.31	0.025	1.09	300	1356	1

Table 3
MTS model parameters of OFHC Cu (Gourdin and Lassila [26]).

Parameters	$g_{0\varepsilon}$	A	p	q	$\hat{\sigma}_{\varepsilon s0}$ [MPa]	α	K/b^3 [MPa]	$\dot{\varepsilon}_{\varepsilon s0}$ [s ⁻¹]	$\dot{\varepsilon}_{0\varepsilon}$ [s ⁻¹]
Copper	1.6	0.235	2/3	1	1100	2	0.823	$5.66 \cdot 10^{10}$	10^7

3.1. The Johnson–Cook model

Johnson et al. [24] proposed a constitutive model for metals subjected to large strains, high strain rates, and high temperatures. This model has enjoyed much success because of its simplicity and because of the availability of parameters for various materials of interest. In the Johnson–Cook model, the flow stress is expressed as:

$$\sigma_y = (A + B\varepsilon^P)^n \left(1 + C \ln \left(\frac{\dot{\varepsilon}}{\dot{\varepsilon}_0} \right) \right) \left(1 - \left(\frac{T - T_0}{T_m - T_0} \right)^m \right) \quad (3.8)$$

The JC flow stress parameters of copper are presented in Table 2.

Where $\dot{\varepsilon}_0$ is a reference strain rate ($\dot{\varepsilon}_0$ is usually taken to be 1 s^{-1}), T , T_0 , and T_m are the current, initial or reference, and melting temperatures, respectively. In the right-hand side of equation (3.8), the first term gives the stress as a function of the strain-hardening coefficient B and the strain hardening exponent n , the second term represents the instantaneous strain rate sensitivity and the last term represents the temperature dependence of flow stress. Here, C is the strain-rate parameter and m is the thermal-softening parameter. The material constant of that material have been identified by Johnson et al. [24].

3.2. The Mechanical Threshold Stress–Dislocation Density model (MTS–DD model)

3.2.1. MTS model

In order to represent correctly the thermoviscoplastic behavior of the work material during machining, the MTS model, written in the form proposed by Follansbee and Kocks [25] and Gourdin and Lassila [26] is introduced here. The model has been investigated by other authors (e.g., Mecking and Kocks [27], Klepaczko and Chiem [28], and Klepaczko [29]). It consists of a description of the material behavior at constant structure and of a description of structure evolution during deformation. These authors attempted to establish a direct relation between dislocation behavior and macroscopic behavior. A reference threshold stress ($\hat{\sigma}$) is employed as the sole internal state variable representing a measure of the hardness of the material at its current dislocation structure. This variable represents an isotropic resistance to plastic flow, which may be related to the dislocation density. The mechanical threshold stress is separated into two components, an athermal stress ($\hat{\sigma}_a$) and a thermal stress ($\hat{\sigma}_t$). Based on this assumption, the following expression is derived for the flow stress [25]:

$$\begin{aligned} \sigma_y &= \hat{\sigma}_a + \hat{\sigma}_t \\ \hat{\sigma}_t &= \hat{\sigma}_D S(\varepsilon^P, T) \end{aligned} \quad (3.9)$$

where $\hat{\sigma}_D$ is the thermal component related to the dislocation and the factor $S(\dot{\epsilon}^p, T)$ is less than 1, so it expresses the dislocation stress, which is lowered due to thermal activation. So, we can write the flow stress in the following form:

$$\sigma_y = \hat{\sigma}_a + \hat{\sigma}_D S(\dot{\epsilon}^p, T) = (\hat{\sigma} - \hat{\sigma}_a) \left(1 - \left(\frac{KT}{g_{0\epsilon} G b^3} \ln \left(\frac{\dot{\epsilon}_{0\epsilon}}{\dot{\epsilon}^p} \right) \right)^{\frac{1}{q}} \right)^{\frac{1}{p}} \tag{3.10}$$

The athermal stress $\hat{\sigma}_a = \frac{0.278}{\sqrt{D}}$, which characterizes the rate-independent interactions of dislocations with long-range barriers, depends on the initial average grain size ($D \approx 50 \mu\text{m}$) as reported in Gourdin and Lassila [26]. In Eq. (3.10), $g_{0\epsilon}$ is the activation energy, $\dot{\epsilon}_{0\epsilon}$ is the reference strain rate, K is the Boltzmann constant, b is the Burgers vector, T is the temperature, and G is the shear modulus. The shape of the obstacle profile is characterized by the constants p and q , $0 \leq p \leq 1$ and $1 \leq q \leq 2$. Equation (3.10) is completed with a hardening law, which takes dislocation accumulation and dynamic recovery into account. Hardening, denoted by θ , is given by:

$$\theta = \frac{d\hat{\sigma}_D}{d\epsilon^p} = \theta_0 (1 - F(X))$$

$$F(X) = \frac{\tanh(\alpha X)}{\tanh(\alpha)}, \quad X = \frac{\hat{\sigma} - \hat{\sigma}_a}{\hat{\sigma}_{\epsilon S} - \hat{\sigma}_a} = \frac{\hat{\sigma}_D}{\hat{\sigma}_{\epsilon S} - \hat{\sigma}_a} \tag{3.11}$$

The initial strain hardening rate θ_0 , due to dislocation accumulation, is expressed as $\theta_0 = 2150 + 0.034\dot{\epsilon}^p$. This expression is found by curve fitting to data obtained for OFHC copper with a similar initial grain size [26]. $\alpha = 2$ is an empirical parameter, $\hat{\sigma}_{\epsilon S}$ is the saturation stress dependent on temperature and sensitive to the strain rate, given by the expression:

$$\hat{\sigma}_{\epsilon S} = \hat{\sigma}_{\epsilon S0} \exp \left(\frac{KT}{G b^3 A} \right) \frac{\dot{\epsilon}_{\epsilon S0}}{\dot{\epsilon}^p} \tag{3.12}$$

$\dot{\epsilon}_{\epsilon S0}$ is constant, A is a dimensionless activation energy, $\hat{\sigma}_{\epsilon S0}$ represents the saturation threshold stress at 0 K and corresponds to the stress at zero work hardening rate.

When metals are subjected to plastic deformation, heat is generated. If the deformations are applied slowly, such as in quasi-static loading conditions, heat is conducted away from the deformed regions and the entire specimen is essentially in an isothermal condition. On the other hand, when deformations are rapidly applied, the process is essentially adiabatic [30]. Thus, for quasi-static loading conditions, we assume isothermal conditions. Concerning dynamic loading, the prediction is made for adiabatic condition. The temperature is calculated assuming that 95% of the work of plastic deformation is converted into heat, which results in a temperature rise given by:

$$\Delta T = \frac{\Omega}{\rho C_p} \int_0^{\bar{\epsilon}^p} \sigma_e d\bar{\epsilon}^p \tag{3.13}$$

where $\Omega = 0.95$ is the Taylor–Quinney coefficient, ρ is the mass density, and C_p is the specific heat.

3.2.2. Dislocation density model (DD)

To predict the microstructure evolution on the specimen during shearing in terms of dislocation density and cell size, the DD model developed by Estrin et al. [17] is introduced. A dislocation cell structure is assumed to form during deformation, which consists of two parts, dislocation cell walls and cell interiors, and obeys a rule of mixtures. Different types of dislocation densities are distinguished in the model: the cell interior dislocation density (ρ_c) and the cell wall dislocation density (ρ_w), which is further divided into two distinct groups: statistical dislocation density (ρ_{ws}) and geometrically necessary dislocation density (ρ_{wg}). The corresponding evolution laws are as follows:

$$\dot{\rho}_c = \alpha^* \frac{1}{\sqrt{3}b} \sqrt{\rho_{ws} + \rho_{wg}} \dot{\gamma}_w^r - \beta^* \frac{6}{bdf(1-f)^{\frac{1}{3}}} \dot{\gamma}_c^r - k_0 \left(\frac{\dot{\gamma}_w^r}{\dot{\gamma}_0} \right)^{\frac{1}{n}} \rho_c \dot{\gamma}_c^r \tag{3.14}$$

$$\dot{\rho}_{ws} = \beta^* \frac{\sqrt{3}(1-f)}{fb} \sqrt{\rho_{ws} + \rho_{wg}} \dot{\gamma}_c^r + (1-\xi)\beta^* \frac{6(1-f)^{\frac{2}{3}}}{fdb} \dot{\gamma}_c^r - k_0 \left(\frac{\dot{\gamma}_w^r}{\dot{\gamma}_0} \right)^{\frac{1}{n}} \rho_{ws} \dot{\gamma}_w^r \tag{3.15}$$

$$\dot{\rho}_{wg} = \xi\beta^* \frac{6(1-f)^{\frac{2}{3}}}{bdf} \dot{\gamma}_c^r \tag{3.16}$$

The first term on the right-hand side of Equations (3.14) and (3.15) corresponds to the generation of dislocations due to the activation of Frank–Read sources. The parameters α^* , β^* , and k_0 are numerical constants, b is the magnitude of the Burgers vector, d is the dislocation cell size. The loss of cell interior dislocations to cell walls where they are ‘woven in’ is accounted for by the second term in Equations (3.14) and (3.15). Finally, the last (negative) term in each one of the evolution

Table 4
DD model parameters of OFHC copper (Ding [34]).

Material	α^*	β^*	K_0	B	$\dot{\gamma}_0^r$	f_0	f_∞	H	M	$\bar{\gamma}^r$	ρ_{w0}	ρ_{c0}	b
Copper	0.04	0.01	12	14,900	4E3	0.25	0.077	10	3.06	3.2	1E7	1E8	2.56E-7

equations represents the annihilation of dislocations leading to dynamic recovery in the course of straining. The density of geometrically necessary dislocations is assumed to arise from a friction ξ of the dislocations coming into cell walls from the cell interiors (see Equation (3.14)), n is a temperature sensitivity parameter that corresponds to recrystallization or annihilation of the dislocation microstructure ($n = \frac{B}{T}$, with B a constant and T a temperature), f is the volume fraction of the dislocation cell wall, $\dot{\gamma}_w^r$ and $\dot{\gamma}_c^r$ are the resolved shear strain rate for the cell walls and interiors, respectively, and $\dot{\gamma}_0^r$ is the reference resolved shear strain rate. It is assumed that the resolved shear strain rates across the cell walls and cell interiors are equal (i.e. $\dot{\gamma}^r = \dot{\gamma}_w^r = \dot{\gamma}_c^r$), which satisfies the strain compatibility along the interface between interiors and boundaries. The resolved shear strain rate can be calculated by the plastic strain rate given by the MTS model with the Taylor factor M as follows:

$$\dot{\gamma}^r = M\dot{\epsilon} \tag{3.17}$$

The coupling of the two models (MTS–DD) is based on the Taylor hypothesis [31]. He proposes a model for the behavior of polycrystals in the form of a hypothesis based on experimental observations. He concludes that the deformation field in polycrystals is homogeneous. This means that each grain deforms exactly as the polycrystal, that is, each grain conforms to the macroscopic stress imposed on the polycrystal.

However, with this hypothesis, the state of the stress is not continuous, but varies abruptly at the grain interfaces and also depends on the orientations of the different grains, so that each grain satisfies the relation (3.17), where M is the Taylor factor, which can vary depending on the texture of the material texture. The value is approximately 3.06 for isotropic polycrystals, such as OFHC Cu.

Since the crystallographic slip of ductile materials causes shearing, which acts on well-defined planes, the nominal value σ of the stress to which the tensile specimen was subjected was not considered, but only the tangential component $\tau = M_\odot\sigma$ (cission stress), which is in the sliding plane and follows the slip direction.

Finally, the proposed coupling of the MTS and DD models is done by the Taylor transformation at each time increment. Knowing the thermo-mechanical state given by the MTS model, then it is possible to evaluate the microstructure evolution with the DD model.

Their evolution with strain governs the overall mechanical threshold stress behavior of the deforming material. The total dislocation density is given by a rule of mixtures:

$$\rho_{tot} = f(\rho_{ws} + \rho_{wg}) + (1 - f)\rho_c \tag{3.18}$$

An important element of the model is the consideration of the evolution of the volume fraction of the cell walls based on experimental observations. According to Muller et al. [32], f decreases with strain monotonically, as the dislocation cell walls become sharper and narrower with strain. The variation of f can be expressed through the following empirical relation [17]:

$$f = f_\infty + (f_0 - f_\infty)e^{\left(\frac{-\dot{\gamma}^r}{\dot{\gamma}^r - \xi}\right)} \tag{3.19}$$

where f_0 is the initial value of f and f_∞ is its saturation value at large strains.

The dislocation cell size d is related to the total dislocation density ρ_{tot} according to Holt’s formula:

$$d = H/\sqrt{\rho_{tot}} \tag{3.20}$$

where the parameter H is about 10 for copper [33].

The process of grain refinement during plastic deformation in the specimen, subjected to large deformation, is assumed to follow a scenario in which the accumulation of misorientations between neighboring dislocation cells with strain gradually converts the dislocation cell structure into a new grain structure. In this study, the average cell size (d) can be identified as the grain size. The process of grain refinement during shearing, subjected to large deformation, is assumed to follow a scenario in which accumulation of misorientations between neighboring dislocation cells with strain gradually converts the dislocation cell structure into a new grain structure. In this study, the average cell size (d) can be identified as the grain size after processing application. The DD model parameters of OFHC copper are presented in Table 4.

4. Result and discussion

In the first part of the test program, the specimens were strained at a constant strain rate $\dot{\epsilon} = 10^{-3} \text{ s}^{-1}$, by using a universal closed-loop machine. All tests were performed up to large strain $\Gamma_{max} \cong 2.5$. Using the SHTB technique, a second

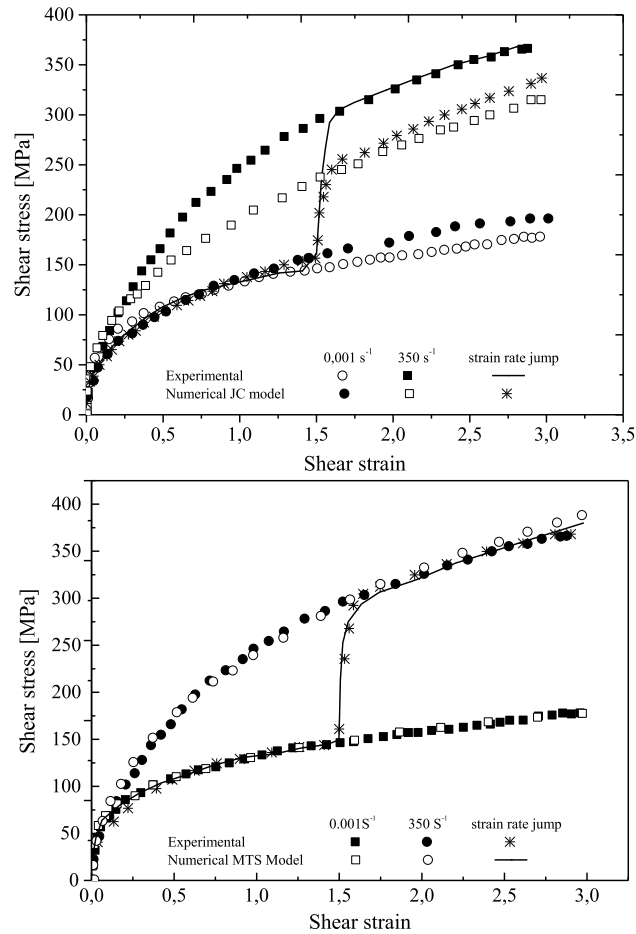


Fig. 4. (a) Comparison between rheological tests data and JC models calculations for OFHC Cu during shearing deformation. (b) Comparison between rheological tests data and MTS models calculations for OFHC Cu during shearing deformation.

series of tests was performed at the nominal strain rate, $\dot{\Gamma} = 350 \text{ s}^{-1}$. Since the maximum shear strain is limited to 0.4, one specimen has to be consecutively loaded from 6 to 8 times to reach the desired large strain $\Gamma_{\max} \cong 2.5$. This method of loading produces practically isothermal stress strain curve at relatively high strain rate. To check this condition of isothermal deformation, numerical calculations were performed using the finite element code Abaqus/Explicit for $\dot{\Gamma} = 350 \text{ s}^{-1}$ up the shear strain equal to 0.4. We assume that the process is adiabatic, the results obtained show that the maximum of rise temperature is attained in the center of the sample, at about 380 K. So, the isothermal process of deformation used in the analysis of the experimental results is justified. Consequently, the other numerical calculations are performed by assuming isothermal conditions.

To study strain history effects, another series of tests were performed at low strain rate ($\dot{\Gamma} = 10^{-3} \text{ s}^{-1}$) up a shear strain equal to $\Gamma \cong 1.5$ and next loaded twice dynamically using the SHTB. Fig. 4a shows the experimental and numerical predictions results of the Johnson–Cook Model for polycrystalline copper. We note a small difference between the quasi-static and dynamic curves at small strain, as found previously by Klepaczko [28]. But with the progress of plastic deformation, the stress difference at the same level of strain substantially increases. For example, when $\Gamma \cong 2.5$, the dynamic curve (Γ , $\tau(\Gamma)$) is twice higher as the quasi-static one. We note also, that each time after two pre-strains the dynamically reloaded curve (Γ , $\tau(\Gamma)$) shows enormous strain hardening θ . The instantaneous response is not detectable within the resolution of the split Hopkinson tensional bar technique. Numerical differentiation of reloaded curves confirmed at a very high value θ (about 4.5×10^3), so the value of θ/G is equal to 0.1 with $G \cong 4.45 \times 10^4 \text{ MPa}$; these results are in good agreement with the literature.

The confrontation of the Johnson–Cook and the experimental results carried out on copper is shown also in Fig. 4a. The solid lines represent the model prediction, while discontinuous lines represent experimental data. We note that the Johnson–Cook model does not correctly predict the behavior of copper at large strain and the strain rate history effect. In fact, numerical calculations show an overshoot when the strain rate is changed from the lower to the higher values. A similar effect is found only for BCC metals [9].

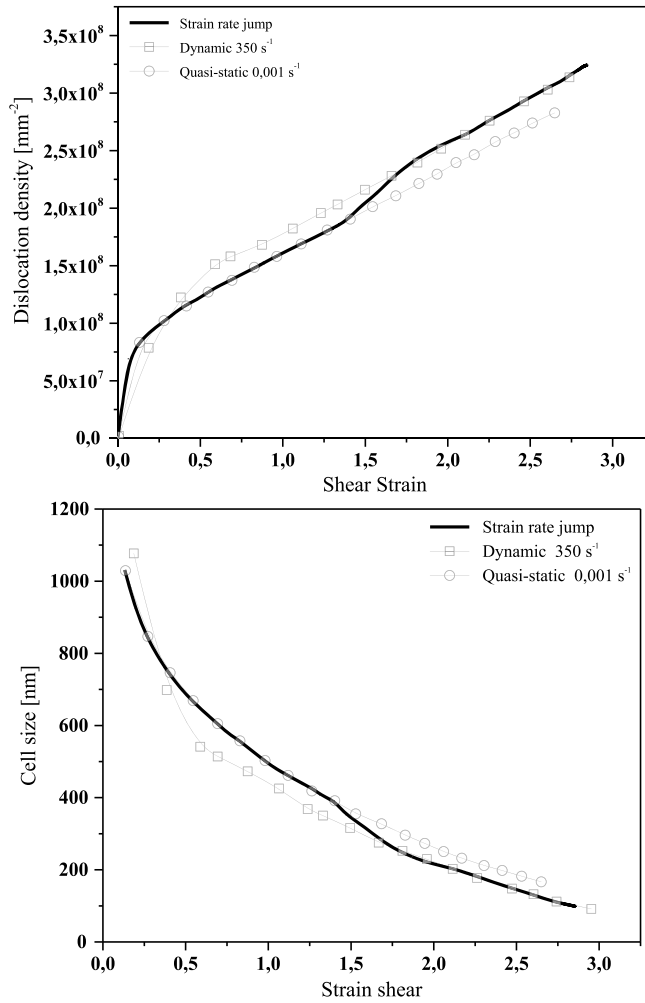


Fig. 5. (a) Simulated developments of the average grain and cell sizes obtained during shearing. (b) Evolution of the average total dislocation densities in the cell.

Fig. 4b illustrates the experimental and numerical predictions results of the MTS model for polycrystalline copper. The MTS model correlation is shown using the solid lines, while the experimental data are shown with discontinuous lines. In this case, the continued straining at the new rate caused the flow shear stress to tend gradually and asymptotically towards the corresponding constant rate. The predictions of the MTS model are in excellent agreement with the measured data.

To understand the strain rate jump process of microstructure dislocation, the dislocation density model is coupled with the MTS model and implemented in the Abaqus software. The obtained results are presented in Fig. 5a. This figure shows the dislocation density as a function of shear deformation for different strain rates. We notice that the dislocation density in the quasi-static case increases, but with a lower rate compared to that of the dynamic case. For a shear strain value 0.3, the gap is zero. This difference increases as the shear strain increases to reach a maximum value 0.2×10^8 . Consequently, more the shear strain is significant, more the cells size formed is weak (see Fig. 5b).

During severe deformation, a significant plastic work appears; this energy is transformed into a form of internal heat. To study the influence of the strain rate jump on temperature generated by the material, we calculated the temperature as a function of the strain rate. Fig. 6 shows the dependence of temperature evolution on the shear strain at different strain rates.

The evolution of the temperature is very high in the adiabatic dynamic case; on the contrary, an isothermal behavior in the quasi-static case is observed. During thermo-mechanical loading, the temperature begins to increase immediately after the strain jump.

5. Conclusion

The understanding of materials deformation and its consequences on the microstructure is critical to achieve accurate materials processing models, especially in the context of manufacturing. This study presents a robust model that can be

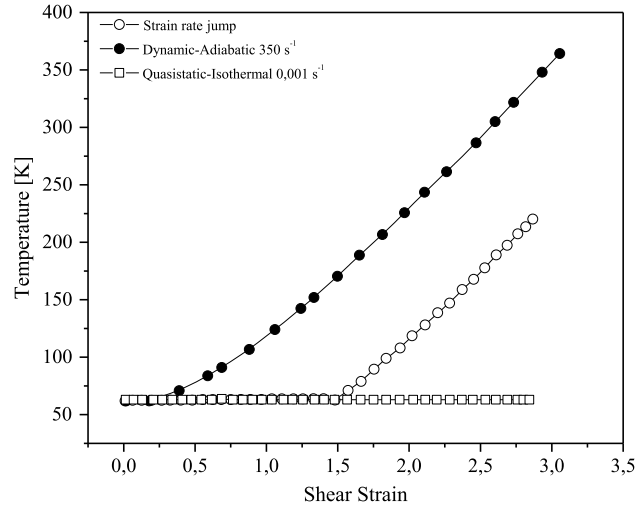


Fig. 6. Simulated evolution of the average temperature.

used for capturing the materials behavior in severe plastic deformation-based process, such as ECAP, machining, forming, etc. A new physics model based on the Materials Threshold Stress (MTS) associated with a Dislocation Density (DD) model is proposed. A set of experiments are performed to determine the quasi-static and dynamic shear–stress behavior of polycrystalline copper (OFHC) at room temperature. In addition to this, strain rate history effects are examined. The new model is compared to the Johnson–Cook empirical model. The Johnson–Cook model demonstrated shortcomings in describing the strain rate history effects. It was not able to give a satisfactory correlation with the experimental response. The proposed model based on the mechanical threshold stress as an internal state variable gave an excellent correlation with experimental data. The model also demonstrated that the microstructure evolution in the context of dislocation densities and the grain size is limited in relation to the strain.

Appendix: Time integration of the combined MTS–DD model

Appendix A. Time integration of the TEVP model (Thermo-Elasto-Visco-Plastic) including the MTS model

The FE (Finite Element) implementation of the TEVP model described in section 3, which includes the MTS hardening model, requires the numerical integration of constitutive equations over a time increment Δt , from a known state at time t_n to the unknown state at t_{n+1} , given the total strain tensor increment $\Delta \boldsymbol{\epsilon}$, and the stress tensor $\boldsymbol{\sigma}$ and state variables \mathbf{y} at t_n . An explicit time integration scheme based on the forward Euler scheme is adopted to implement the TEVP model in Abaqus/Explicit FE software via the user subroutine VUMAT. The forward Euler scheme allows direct calculation (i.e. without iterative calculation) over Δt . The forward Euler scheme is efficient when Δt is small enough, so time derivatives involving in the TEVP model could be evaluated by the known variables at t_n . This is the case in the FE simulation of the severe deformation process in the Abaqus/Explicit code, where Δt is small enough to consider derivatives at t_n when assessing increments of state variables.

The algorithm assumes an elastic behavior prediction and a plastic behavior correction (when required). Giving $\Delta \boldsymbol{\epsilon}$, $\boldsymbol{\sigma}_n$ et \mathbf{y}_n , the elastic state over Δt is calculated by:

$$\Delta \boldsymbol{\sigma}^{\text{trial}} = \mathbf{C} : \Delta \boldsymbol{\epsilon} \quad (\text{A.1})$$

and elastic stress state at the end of increment is:

$$\boldsymbol{\sigma}_{n+1}^{\text{trial}} = \boldsymbol{\sigma}_n + \Delta \boldsymbol{\sigma}^{\text{trial}} \quad (\text{A.2})$$

In this case, hardening state variables did not evolve (increment of state variables $\Delta \mathbf{y} = \mathbf{0}$), since loading is assumed purely elastic ($\Delta \boldsymbol{\epsilon}^p = \mathbf{0}$ since there is no plastic strain, and $\Delta \boldsymbol{\epsilon}^{\text{th}} = \mathbf{0}$ since there is no temperature increase due to plastic strain). Hence, the internal state variables associated with plastic deformation do not evolve, so:

$$\mathbf{y}_{n+1} = \mathbf{y}_n \quad (\text{A.3})$$

Then, by checking the sign of the yield criterion:

$$\text{sign}[F(\boldsymbol{\sigma}_{n+1}, \mathbf{y}_n) = \bar{\sigma}(\boldsymbol{\sigma}_{n+1}) - \sigma_y(\mathbf{y}_n)] \quad (\text{A.4})$$

Table A.1

Time integration, based on forward Euler scheme, of the TEVP model, including the MTS hardening model.

Input data: $\Delta \boldsymbol{\varepsilon}$, $\boldsymbol{\sigma}_n$, $\bar{\varepsilon}_n^p$ and \mathbf{y}_n
Elastic prediction $\Delta \boldsymbol{\sigma}^{\text{trial}} = \mathbf{C} : \Delta \boldsymbol{\varepsilon}$, $\boldsymbol{\sigma}_{n+1}^{\text{trial}} = \boldsymbol{\sigma}_n + \Delta \boldsymbol{\sigma}^{\text{trial}}$
Check yield criterion $\text{sign}[F(\boldsymbol{\sigma}_{n+1}, \mathbf{y}_n) - \bar{\sigma}(\boldsymbol{\sigma}_{n+1}) - \sigma_y(\mathbf{y}_n)]$
1. If $\text{sign} < 0$, then the loading is purely elastic $\Delta \boldsymbol{\sigma} = \Delta \boldsymbol{\sigma}^{\text{trial}}$, $\Delta \mathbf{y} = 0$, $\Delta \bar{\varepsilon}^p = \Delta \lambda = 0$
2. Else the loading is elastoplastic $\mathbf{V}_n = \left. \frac{\partial F}{\partial \boldsymbol{\sigma}} \right _n$, $\Delta \bar{\varepsilon}^p = \Delta \lambda = \frac{\mathbf{V}_n : \mathbf{C} : \Delta \boldsymbol{\varepsilon}}{H_{\lambda n}}$, $\Delta \boldsymbol{\varepsilon}^p = \mathbf{V}_n \Delta \lambda$ $\Delta \boldsymbol{\sigma} = \mathbf{C} : (\Delta \boldsymbol{\varepsilon} - \Delta \boldsymbol{\varepsilon}^p)$, $\Delta \mathbf{y} = \Delta \lambda \mathbf{h}(\boldsymbol{\sigma}_n, \mathbf{y}_n)$
Update variables $\boldsymbol{\sigma}_{n+1} = \boldsymbol{\sigma}_n + \Delta \boldsymbol{\sigma}$, $\mathbf{y}_{n+1} = \mathbf{y}_n + \Delta \mathbf{y}$, $\bar{\varepsilon}_{n+1}^p = \bar{\varepsilon}_n^p + \Delta \bar{\varepsilon}^p$ Return $\boldsymbol{\sigma}_{n+1}$, $\bar{\varepsilon}_{n+1}^p$ and \mathbf{y}_{n+1}

if $\text{sign} < 0$ then the loading over Δt is effectively elastic, so

$$\begin{aligned} \boldsymbol{\sigma}_{n+1} &= \boldsymbol{\sigma}_{n+1}^{\text{trial}} \\ \mathbf{y}_{n+1} &= \mathbf{y}_n \\ \bar{\varepsilon}_{n+1}^p &= \bar{\varepsilon}_n^p \end{aligned} \tag{A.5}$$

By cons, if $\text{sign} > 0$, there is a plastic loading and the state should be updated, including work hardening. In this case, first the plastic flow direction is calculated at t_n , as

$$\mathbf{V}_n = \left. \frac{\partial F}{\partial \boldsymbol{\sigma}} \right|_n = \frac{3}{2} \frac{\boldsymbol{\sigma}'_n}{\bar{\sigma}_n} \tag{A.6}$$

Then, the equivalent plastic strain increment is calculated as follows:

$$\Delta \bar{\varepsilon}^p = \Delta \lambda = \frac{\mathbf{V}_n : \mathbf{C} : \Delta \boldsymbol{\varepsilon}}{H_{\lambda n}} \tag{A.7}$$

So that $H_{\lambda n}$ is calculated as:

$$H_{\lambda n} = \mathbf{V}_n : \mathbf{C} : \mathbf{V}_n + H_{\sigma_y n} = 2G|\mathbf{V}_n|^2 + H_{\sigma_y n} \tag{A.8}$$

Given that $|\mathbf{V}_n| = \sqrt{V_{ij}V_{ij}} = \sqrt{\frac{3}{2}}$, $H_{\lambda n}$ becomes:

$$H_{\lambda n} = 3G + H_{\sigma_y n} \tag{A.9}$$

For the MTS model, $H_{\sigma_y n}$, given by Eq. (3.11), is evaluated with known variables at t_n : The plastic strain tensor increment is then calculated as:

$$\Delta \boldsymbol{\varepsilon}^p = \mathbf{V}_n \Delta \lambda \tag{A.10}$$

The thermal strain tensor is calculated as follows:

$$\Delta \boldsymbol{\varepsilon}^{\text{th}} = \alpha \Delta T \cdot \mathbf{I} \tag{A.11}$$

The stress tensor increment $\Delta \boldsymbol{\sigma}$ is then calculated as:

$$\Delta \boldsymbol{\sigma} = \mathbf{C} : (\Delta \boldsymbol{\varepsilon} - \Delta \boldsymbol{\varepsilon}^p - \Delta \boldsymbol{\varepsilon}^{\text{th}}) \tag{A.12}$$

The stress tensor, state variables and equivalent plastic strain are updated as follows:

$$\begin{aligned} \boldsymbol{\sigma}_{n+1} &= \boldsymbol{\sigma}_n + \Delta \boldsymbol{\sigma} \\ \mathbf{y}_{n+1} &= \mathbf{y}_n + \Delta \mathbf{y} \\ \bar{\varepsilon}_{n+1}^p &= \bar{\varepsilon}_n^p + \Delta \bar{\varepsilon}^p \end{aligned} \tag{A.13}$$

Appendix B. Time integration of the DD model

Using updated state variable from time integration of the TEVP model, including the MTS model, it is possible to estimate physical quantities (i.e. dislocations density, grain size) related to the microstructure evolution during cutting.

According to Eqs. (3.14), (3.15), and (3.17), it is possible to write dislocation densities rates in the following forms:

$$\dot{\rho}_c = \Gamma_c \dot{\gamma}^r = \Gamma_c M \dot{\varepsilon} \quad (\text{B.1})$$

$$\dot{\rho}_{ws} = \Gamma_{ws} \dot{\gamma}^r = \Gamma_{ws} M \dot{\varepsilon} \quad (\text{B.2})$$

$$\dot{\rho}_{wg} = \Gamma_{wg} \dot{\gamma}^r = \Gamma_{wg} M \dot{\varepsilon} \quad (\text{B.3})$$

with

$$\begin{aligned} \Gamma_c &= \Gamma_c(f, d, \rho_c, \rho_{ws}, \rho_{wg}) \\ &= \alpha^* (1/\sqrt{3}b) \sqrt{\rho_{ws} + \rho_{wg}} - 6\beta^* (bdf(1-f)^{1/3})^{-1} - k_0 (\dot{\gamma}_w^r / \dot{\gamma}_0)^{-1/n} \rho_c \end{aligned} \quad (\text{B.4})$$

$$\begin{aligned} \Gamma_{ws} &= \Gamma_{ws}(f, d, \rho_{ws}, \rho_{wg}) \\ &= \beta^* (\sqrt{3}(1-f)/fb) \sqrt{\rho_{ws} + \rho_{wg}} + (1-\xi)\beta^* (6(1-f)^{2/3}/bdf) - k_0 (\dot{\gamma}_w^r / \dot{\gamma}_0)^{-1/n} \rho_{ws} \end{aligned} \quad (\text{B.5})$$

$$\Gamma_{wg} = \xi\beta^* (6(1-f)^{2/3}/bdf) \quad (\text{B.6})$$

Over a time increment Δt , it is possible to write these ODEs using Euler's forward integration scheme, in the following form:

$$\Delta \rho_c = \Gamma_c|_{t+\Delta t} \Delta \gamma^r = \Gamma_c|_{t+\Delta t} M \Delta \varepsilon \quad (\text{B.7})$$

$$\Delta \rho_{ws} = \Gamma_{ws}|_{t+\Delta t} \Delta \gamma^r = \Gamma_{ws}|_{t+\Delta t} M \Delta \varepsilon \quad (\text{B.8})$$

$$\Delta \rho_{wg} = \Gamma_{wg}|_{t+\Delta t} \Delta \gamma^r = \Gamma_{wg}|_{t+\Delta t} M \Delta \varepsilon \quad (\text{B.9})$$

The increment of dislocation densities ρ_{ws} and ρ_{wg} are then deduced to:

$$\rho_c|_{t+\Delta t} = \rho_c|_t + \Delta \rho_c \quad (\text{B.10})$$

$$\rho_{ws}|_{t+\Delta t} = \rho_{ws}|_t + \Delta \rho_{ws} \quad (\text{B.11})$$

$$\rho_{wg}|_{t+\Delta t} = \rho_{wg}|_t + \Delta \rho_{wg} \quad (\text{B.12})$$

The total dislocation density, given by the rule of mixtures (3.18), is then calculated by:

$$\rho_{\text{tot}}|_{t+\Delta t} = f|_{t+\Delta t} (\rho_{ws}|_{t+\Delta t} + \rho_{wg}|_{t+\Delta t}) + (1-f|_{t+\Delta t}) \rho_c|_{t+\Delta t} \quad (\text{B.13})$$

with

$$f|_{t+\Delta t} = f_\infty + (f_0 - f_\infty) e^{(-\gamma^r|_{t+\Delta t} / \bar{\gamma}^r)} \quad (\text{B.14})$$

where

$$\gamma^r|_{t+\Delta t} = \gamma^r|_t + \Delta \gamma^r = \gamma^r|_t + M \Delta \varepsilon \quad (\text{B.15})$$

From Eq. (B.13), the average grain size is then estimated, using Eq. (3.20), by:

$$d|_{t+\Delta t} = H / \sqrt{\rho_{\text{tot}}|_{t+\Delta t}} \quad (\text{B.16})$$

Appendix C. Implantation of the MTS model – integration over a time increment

1. Model parameters

$$g_{0i}, A, p, q, \hat{\sigma}_{Ds0}, \alpha, \frac{K}{b^3}, \dot{\varepsilon}_{Ds0}, \dot{\varepsilon}_{0D}, E, \mu, \rho, C_p, \vartheta. \quad (\text{C.1})$$

2. Initialization at the first increment

$$\Delta \varepsilon, \sigma_{y(0)} = \hat{\sigma}_a = \frac{0.278}{\sqrt{D}}, \bar{\varepsilon}_0^p = 0, \Delta \bar{\varepsilon}_p = 0, T_n = T_{\text{ref}}, \hat{\sigma}_{D(0)} = 0, \hat{\sigma}_{Ds(0)} = 0 \quad (\text{C.2})$$

3. Increment start

$$\Delta t, \Delta \varepsilon, \sigma_{y(n)}, \bar{\varepsilon}_n^p, T_n, \Delta \bar{\varepsilon}_n^p, \hat{\sigma}_{D(n)}, \hat{\sigma}_{Ds(n)} \quad (\text{C.3})$$

4. Elastic state test

- Elastic test stress calculated on a time increment Δt :

$$\Delta\sigma^{\text{trial}} = C : \Delta\varepsilon \tag{C.4}$$

- The stress tensor at the end of the increment is:

$$\sigma_{n+1}^{\text{trial}} = \sigma_n + \Delta\sigma^{\text{trial}} \tag{C.5}$$

- Then, by verifying the threshold surface function sign

$$\text{sign}[F = \bar{\sigma}(\sigma_{n+1}^{\text{trial}}) - \sigma_{y(n)}] \tag{C.6}$$

- If ($\text{sign} \leq 0$), the loading is elastic on the increment Δt :

$$\sigma_{n+1} = \sigma_{n+1}^{\text{trial}} \tag{C.7}$$

$$\bar{\varepsilon}_{n+1}^p = \bar{\varepsilon}_n^p \tag{C.8}$$

$$\Delta\bar{\varepsilon}_{n+1}^p = 0 \tag{C.9}$$

$$\sigma_{y(n+1)} = \sigma_{y(n)} \tag{C.10}$$

$$T_{n+1} = T_n \tag{C.11}$$

5. Plastic state

If ($\text{sign} < 0$), then the loading is plastic.

- Calculation of the plastic multiplier:

$$\Delta\bar{\varepsilon}_p = \frac{\sigma(\sigma_{n+1}^{\text{trial}}) - \sigma_{y(n)}}{3\mu + \theta_n} \approx \frac{\sigma(\sigma_{n+1}^{\text{trial}}) - \sigma_{y(n)}}{3\mu} \text{ since } \theta_n \ll 3\mu \tag{C.12}$$

- Calculation of the plastic deformation:

$$\bar{\varepsilon}_{n+1}^p = \bar{\varepsilon}_n^p + \Delta\bar{\varepsilon}_p \tag{C.13}$$

- Calculation of the deformation rate:

$$\dot{\bar{\varepsilon}}_p = \frac{\Delta\bar{\varepsilon}_p}{\Delta t} \tag{C.14}$$

- Calculation of the flow stress:

o Saturation stress $\hat{\sigma}_{Ds}$:

$$\hat{\sigma}_{Ds(n+1)} = \hat{\sigma}_{Ds0} \exp\left(\frac{KT_n}{\mu b^3 A}\right) \frac{\dot{\bar{\varepsilon}}_{Ds0}}{\dot{\bar{\varepsilon}}_p} \tag{C.15}$$

o The thermal stress related to dislocations from the hardening function $\hat{\sigma}_D$ is:

$$\theta_0 = 2150 + 0.034\dot{\bar{\varepsilon}}_p \tag{C.16}$$

$$X_n = \frac{\hat{\sigma}_{D(n)}}{\hat{\sigma}_{Ds(n)} - \hat{\sigma}_a} \tag{C.17}$$

$$\theta_n = \theta_0 \left[1 - \frac{\tan(\alpha X_n)}{\tan(\alpha)} \right] \tag{C.18}$$

$$\Delta\hat{\sigma}_D = \theta_n \Delta\bar{\varepsilon}_p \tag{C.19}$$

$$\hat{\sigma}_{D(n+1)} = \hat{\sigma}_{D(n)} + \Delta\hat{\sigma}_D \tag{C.20}$$

- Flow stress:

$$S_{D(n)} = \left[1 - \left(\frac{KT_n}{g_{0i}\mu b^3} \ln \frac{\dot{\bar{\varepsilon}}_{0D}}{\dot{\bar{\varepsilon}}_p} \right)^{\frac{1}{q}} \right]^{\frac{1}{p}} \tag{C.21}$$

$$\sigma_{y(n+1)} = \hat{\sigma}_a + S_{D(n)}\hat{\sigma}_{D(n)} \tag{C.22}$$

- Stress tensor:

$$\sigma_{n+1} = \sigma_{n+1}^{\text{trial}} - \frac{3\mu\Delta\bar{\epsilon}_p}{\bar{\sigma}_n} \sigma'_n \quad (\text{C.23})$$

- Temperature calculation (adiabatic test):

$$T_{n+1} = T_n + \frac{n_p}{\rho C_p} \bar{\sigma}_n \Delta\bar{\epsilon}_p \quad (\text{C.24})$$

References

- [1] A. Svoboda, D. Wedberg, L.E. Lindgren, Simulation of metal cutting using a physically based plasticity model, *Model. Simul. Mater. Sci. Eng.* 18 (7) (2010) 075005.
- [2] V. Lemiale, Y. Estrin, H.S. Kim, R. O'Donnell, Grain refinement under high strain rate impact: a numerical approach, *Comput. Mater. Sci.* 48 (1) (2010) 124–132.
- [3] G. Rotella, D. Umbrello, Finite element modeling of microstructural changes in dry and cryogenic cutting of Ti₆Al₄V alloy, *CIRP Ann.* 63 (1) (2014) 69–72.
- [4] J.I. Castillo, D.J. Celentano, M.A. Cruchaga, C.M. García-Herrera, Characterization of strain rate effects in sheet laser forming, *C. R. Mecanique* 346 (2018) 794–805.
- [5] M.B. Bettaieb, F. Abed-Meraim, Strain localization analysis for planar polycrystals based on bifurcation theory, *C. R. Mecanique* 346 (8) (2018) 647–664.
- [6] N.S. Nguyen, H. Magoaric, B. Cambou, Analysis of local behaviour in granular materials, *C. R. Mecanique* 342 (3) (2014) 156–173.
- [7] U.S. Lindholm, Some experiments with the split Hopkinson pressure bar, *J. Mech. Phys. Solids* 12 (5) (1964) 317–335.
- [8] U.S. Lindholm (Ed.), *Mechanical Behavior of Materials Under Dynamic Loads*, Symposium Held in San Antonio, TX, USA, 6–8 September 1967, Springer-Verlag, New York, 1968.
- [9] Z.N. Mao, X.H. An, X.Z. Liao, J.T. Wang, Opposite grain size dependence of strain rate sensitivity of copper at low vs high strain rates, *Mater. Sci. Eng. A* 738 (2018) 430–438.
- [10] T. Zhang, K. Zhou, Z.Q. Chen, Strain rate effect on plastic deformation of nanocrystalline copper investigated by molecular dynamics, *Mater. Sci. Eng. A, Struct. Mater.: Prop. Microstruct. Process.* 648 (2015) 23–30.
- [11] W. Chen, T. Kitamura, M. Feng, Effect of geometrically necessary dislocations on inelastic strain rate for torsion stress relaxation of polycrystalline copper in micro scale, *Mater. Sci. Eng. A, Struct. Mater.: Prop. Microstruct. Process.* 726 (2018) 137–142.
- [12] S.-h. Huang, D.-y. Shu, C.-k. Hu, S.-f. Zhu, Effect of strain rate and deformation temperature on strain hardening and softening behavior of pure copper, *Trans. Nonferr. Met. Soc. China* 26 (4) (2016) 1044–1054.
- [13] B. Jiang, S. Zhang, The effects of strain rate and grain size on nanocrystalline materials: a theoretical prediction, *Mater. Des.* 87 (2015) 49–52.
- [14] P.E. Senseny, J. Duffy, R.H. Hawley, Experiments on strain rate history and temperature effects during the plastic deformation of close-packed metals, *J. Appl. Mech.* 45 (1) (1978) 60–66.
- [15] A.B. Tanner, D.L. McDowell, Deformation temperature and strain rate sequence experiments on OFHC Cu, *Int. J. Plast.* 15 (1999) 375–399.
- [16] A.B. Tanner, R.D. McGinty, D.L. McDowell, Modeling temperature and strain rate history effects on OFHC Cu, *Int. J. Plast.* 15 (1999) 575–603.
- [17] Y. Estrin, L.S. Toth, A. Molinari, Y. Bréchet, A dislocation-based model for all hardening stages in large strain deformation, *Acta Mater.* 46 (1998) 5509–5522.
- [18] Y. Estrin, H.S. Kim, Modelling microstructure evolution toward ultrafine crystallinity produced by severe plastic deformation, *J. Mater. Sci.* 42 (2007) 1512–1516.
- [19] Y. Estrin, A. Molotnikov, C.H.J. Davies, R. Lapovok, Strain gradient plasticity modelling of high-pressure torsion, *J. Mech. Phys. Solids* 56 (2008) 1186–1202.
- [20] D.J. Lee, E.Y. Yoon, D.H. Ahn, B.H. Park, H.W. Park, L.J. Park, Y. Estrin, H.S. Kim, Dislocation density-based finite element analysis of large strain deformation behavior of copper under high-pressure torsion, *Acta Mater.* 76 (2014) 281–293.
- [21] V. Lemiale, Y. Estrin, H.S. Kim, R. O'Donnell, Grain refinement under high strain rate impact: a numerical approach, *Comput. Mater. Sci.* 48 (2010) 124–132.
- [22] M. Bacca, D.R. Hayhurst, R.M. McMeeking, Continuous dynamic recrystallization during severe plastic deformation, *Mech. Mater.* 90 (2015) 148–156.
- [23] M. Zenasni, *Caractérisation expérimentale et modélisation du comportement du cuivre en grande déformation: sensibilité à la vitesse*, Ph.D. Thesis, University of Metz, France, 1992.
- [24] G.R. Johnson, W.H. Cook, in: *Proc. 7th International Symposium on Ballistics*, The Hague, The Netherlands, 1983, pp. 12–21.
- [25] P.S. Follansbee, U.F. Kocks, A constitutive description of the deformation of copper based on the use of the mechanical threshold as an internal state variable, *Acta Metall.* 36 (1) (1988) 81–93.
- [26] W.H. Gourdin, D.H. Lassila, Flow stress of OFE copper at strain rates from 10⁻³ to 104 s⁻¹: grain-size effects and comparison to the mechanical threshold stress model, *Acta Metall. Mater.* 39 (1991) 2337–2348.
- [27] H. Mecking, U.F. Kocks, Kinetics of flow and strain-hardening, *Acta Metall.* 29 (1981) 1865–1875.
- [28] J.R. Klepaczko, C.Y. Chiem, On the sensitivity of f.c.c. metals, instantaneous rate sensitivity and rate sensitivity of strain Hardening, *J. Mech. Phys. Solids* 34 (1986) 29–54.
- [29] J.R. Klepaczko, Discussion of microstructural effects and their modeling at high rates of strain, *Inst. Phys. Conf. Ser.* 102 (1988) 283.
- [30] O. Oussouaddi, J.R. Klepaczko, Analysis of transition between the isothermal and adiabatic deformation in the case of torsion of a tube, *J. Phys. IV* 1, 323–334.
- [31] G.I. Taylor, C.F. Elam, Bakerian lecture: The distortion of an aluminium crystal during a tensile test, *Proc. R. Soc. Lond. A, Math. Phys. Eng. Sci.* 102 (1923) 643–667.
- [32] M. Muller, M. Zehetbauer, A. BorbCly, T. Ungcir, Stage IV work hardening in cell forming materials, part I: features of the dislocation structure by X-ray line broadening, *Scr. Mater.* 35 (1996) 1461–1466.
- [33] D.L. Holt, Dislocation cell formation in metals, *J. Appl. Phys.* 41 (1970) 3197.
- [34] H. Ding, N. Shen, Y.C. Shin, Modeling of grain refinement in aluminum and copper subjected to cutting, *Comput. Mater. Sci.* 50 (10) (2011) 3016–3025.